Observing posteruptive deflation of hydrothermal system using InSAR time series analysis: An application of ALOS-2/PALSAR-2 data on the 2015 phreatic eruption of Hakone volcano, Japan

by R. Doke[1], K. Mannen[1], and K. Itadera[1]

[1] Hot Springs Research Institute of Kanagawa Prefecture, 586 Iriuda, Odawara, Kanagawa 250-0031, Japan.

Corresponding author: Ryosuke Doke (r-doke@onken.odawara.kanagawa.jp)

Key Points:

- Posteruptive deflation beneath the central cones of Hakone volcano was detected by radar interferometry after the 2015 phreatic eruption
- Our model inversion suggests that deflation of a hydrothermal system confined by a sealing layer beneath the volcano has been taking place
- The hydrothermal system deflation is likely attributable to rupture of the sealing layer and system depressurization due to the eruption

Abstract

From 29 June to 1 July, 2015, a phreatic eruption occurred in Owakudani, the largest fumarole area in Hakone volcano, Japan. In this study, an interferometric synthetic aperture radar (InSAR) time series analysis of the Advanced Land Observing Satellite-2 (ALOS-2)/Phased Array type L-band Synthetic Aperture Radar-2 (PALSAR-2) data was performed to detect posteruptive deflation after the eruption. The results show that the central cones of the volcano have subsided since the eruption and its deflation source is located beneath the previously estimated bell-shaped conductor, which is considered as a sealing layer confining a pressurized hydrothermal reservoir. Therefore, the InSAR results demonstrate the deflation of the hydrothermal system beneath the volcano. One possible cause of this deflation is compaction due to a decrease in pore pressure caused by rupture and fluid migration during and after the eruption.

Plain Language Summary

From 29 June to 1 July, 2015, an eruption occurred in Owakudani, the largest steaming area in Hakone volcano, Japan. Our analysis using satellite radar demonstrates that the central part of Hakone volcano has subsided since the eruption and that the deflation source is located in the reservoir of hot water beneath the volcano. One possible cause of this deflation is compaction due to a pressure drop produced by rupture and fluid migration during and after the eruption.

1 Introduction

Measurements of crustal deformation in volcanic regions play an important role in volcano monitoring. With the recent development of synthetic aperture radar (SAR) technology, posteruptive deflation has been observed after phreatic eruptions in various volcanoes (e.g., Hamling et al., 2016; Himematsu et al., 2020; Narita & Murakami, 2018). Volcanic deflation, which occurs at different temporal and spatial scales, is explained by various factors, such as decreases in pore pressure resulting from fluid migration (e.g., Todesco et al., 2014; Wang et al., 2019) and thermoelastic responses with cooling (e.g., Furuya, 2005; Wang & Aoki, 2019). Constraining the source of posteruptive deflation is important when evaluating the structure and physical properties of hydrothermal systems beneath volcanoes and assessing the risk of future phreatic eruptions and signals during volcanic unrest. However, the relationship between the deflation source and the structure of the hydrothermal system based on preexisting subsurface surveys has not been sufficiently discussed in previous studies. Recent magnetotelluric surveys have revealed the structure of the hydrothermal system beneath Hakone volcano, the focal point of this study, providing an appropriate context within which to discuss this topic.

Hakone is a caldera volcano located approximately 100 km west of Tokyo, the capital of Japan (Figure 1). This volcano has been active for more than 400 ky, and effusive eruptions of andesitic magma in the past 40 ky have formed its central cones (CCs) (e.g., Mts. Kamiyama and Komagatake in Figure 1) (Geological Society of Japan, 2007). Since its latest magmatic eruption (3 ka), several phreatic eruptions have occurred near Owakudani, the largest fumarole area of the volcano, which was formed on the foot of the latest edifice (Kobayashi et al., 2006; Kobayashi, 2008; Tsuchiya et al., 2017). Since the beginning of the 21st century, volcanic unrest has occurred every few years. The unrest that began in April 2015 was the largest in terms of seismicity in the history of modern observation since 1960. The 2015 unrest culminated in a small phreatic eruption on 29 June in Owakudani, which released 80–130 tons of ash and

ballistic clasts (Furukawa et al., 2015). Although the 2015 phreatic eruption was small in scale, a dense network of instrumental observation sites detected detailed processes of earthquake activity and crustal deformation during the unrest (e.g., Harada et al., 2018; Honda et al., 2018; Yukutake et al., 2017).

The observation during the preeruptive unrest suggests a deep (>6 km) supply of fluid, which was detected as an inflation of the volcanic edifice and a swarm of deep low-frequency events, initiated in early April 2015 (Harada et al., 2018; Yukutake et al., 2019). Then shallow (<6 km) pressurization of the hydrothermal system was implied from an earthquake swarm that occurred beneath the CCs from the end of April, and abnormal steaming activity from a steam production well (SPW) in Owakudani (500 m deep with a well mouth elevation of 1000 m) occurred in early May (Mannen et al., 2018; Yukutake et al., 2017). The area within 200 m of the SPW showed local swelling, which was detected by an interferometric SAR (InSAR) analysis of Advanced Land Observing Satellite-2 (ALOS-2)/Phased Array type L-band Synthetic Aperture Radar-2 (PALSAR-2) data (Doke et al., 2018; Kobayashi et al., 2018). The phreatic eruption occurred near the southern edge of the swelling area from 29 June to 1 July 2015 (Kobayashi et al., 2018). The InSAR analysis of ALOS-2/PALSAR-2 pairs before and after the phreatic eruption has demonstrated surface displacements caused by the opening of an NW–SE-trending crack formed deeper than 830 m above sea level and the closing of a sill beneath the crack, approximately 225 m above sea level (Doke et al., 2018). Although InSAR has poor time resolution, Honda et al. (2018) also estimated an NW–SE-trending crack from a rapid tilt change over the course of 2 min starting at 07:33 JST on 29 June 2015. These lines of evidence indicate that the phreatic eruption was triggered by hydrothermal fluids stored approximately 225 m above sea level, which migrated toward the shallower part of the edifice through the crack during the eruption. Since the 2015 phreatic eruption, fumarolic activity in Owakudani has been higher than before (Mannen et al., 2021). This higher steaming activity during and after the eruption suggests the rupturing of the sealed and pressured hydrothermal system beneath the volcano during the 2015 eruption, as indicated by general modeling of hydrothermal systems (e.g., Fournier, 1999; Stix & de Moor, 2018).

Regarding the location of Hakone volcano, there are residential areas within 1 km of Owakudani, the possible eruption center, so even a small-scale eruption would cause significant damage. Although forecasting phreatic eruptions is known to be challenging, it may be possible to monitor the hydrothermal system located in the shallow regions of the volcano using InSAR. In this study, we performed an InSAR time series analysis of the ALOS-2/PALSAR-2 data to clarify the surface velocities after the 2015 phreatic eruption of Hakone volcano. Applying the inversion technique to the surface velocities, we modeled the deflation sources, and the cause of this deflation is discussed here.

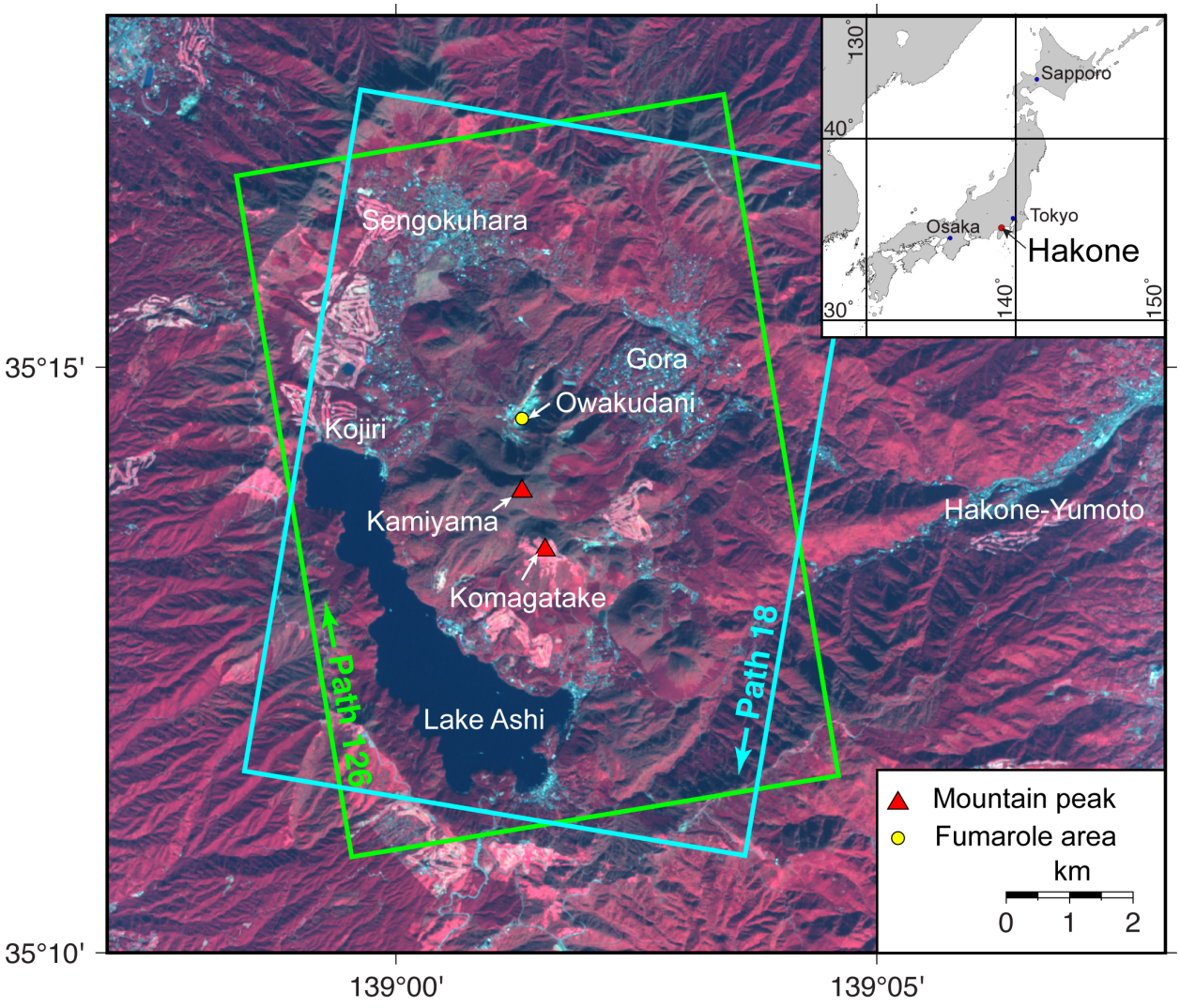

Figure 1. Index map of Hakone volcano. The base map is a false-color image captured by ALOS/AVNIR-2 on 10 November 2006, and the red tones indicate vegetated areas. The areas enclosed by the rectangles indicate the analysis areas in this study.

2 Data and Methods

The PALSAR-2 is a multi-mode and right- and left-looking SAR sensor aboard the ALOS-2 launched by the Japan Aerospace Exploration Agency (JAXA) (Rosenqvist et al., 2014). Its wavelength is 23.8 cm (L-band). The datasets selected for this study are path 126 (ascending orbit, right-looking) and path 18 (descending orbit, right-looking), which include observations of Hakone volcano. These paths have the largest number of observation data of any ascending or descending orbit, respectively, from 2 July 2015 to 1 April 2021, which is the period after the phreatic eruption. Thus, it is expected that many interference pairs can be obtained, allowing for greater precision in the analysis. Paths 126 and 18 represent observations from the west and east sides of the sky, respectively, and their off-nadir angles are 38.7° and

38.9°, respectively. The data extracted for this study are given in Table S1. InSAR time series analysis based on the small baseline subset (SBAS) method (Berardino et al., 2002) was used to remove noise, such as atmospheric effects. For the SBAS-InSAR time series analysis, interference pairs, whose time intervals are within 365 days, were extracted for each path. Path 126 has 21 extracted scenes and 74 pairs, whereas path 18 has 24 extracted scenes and 85 pairs. The time–position plots are shown in Figure S1.

ENVI SARscape software was used for the SBAS-InSAR time series analysis. The analysis area was cut out from the original data to focus on Hakone volcano and reduce the analysis time (Figure 1). The data were averaged over 11 by 14 looks in the range and azimuth directions, respectively (corresponding to an area of approximately 25 m by 25 m), to improve the signal-to-noise ratio. The influence of the topography in initial interferograms was removed using ellipsoidal height, generated from a 10-m digital elevation model (DEM) released by the Geospatial Information Authority of Japan and Earth Gravitational Model 2008 geoid heights (Pavlis et al., 2012). An adaptive filter (Goldstein and Werner, 1998) was used to reduce the noise, and the interferograms were unwrapped by the minimum-cost flow approach (Costantini, 1998) with a 0.2 coherence threshold. For the removal of orbital residuals, 150 points of ground control point were set as good coherence points in the area, except at the CCs of Hakone volcano, in which significant displacements were observed, and a polynomial surface was assumed. For the inversion of the SBAS-InSAR time series analysis (Berardino et al., 2002), a linear displacement model was used. Atmospheric effects were eliminated by applying a spatial low-pass filter with a cutoff of 1,200 m and a temporal high-pass filter with a cutoff of 365 days. Finally, the estimated surface velocities were geocoded to the geographic coordinates in WGS-84, and surface velocity maps were obtained with a resolution of 25 m by 25 m.

3 Results

Figure 2 shows surface velocity maps after the 2015 phreatic eruption estimated by the SBAS-InSAR time series analysis. The velocities are indicated in the line-of-sight (LOS) directions, and positive and negative values indicate velocities toward and away from the satellite, respectively. An area of 2 km in diameter, located at the CCs of the volcano, shows velocities in the negative LOS direction along both paths 126 and 18 (Figure 2). Moreover, these velocities are below −10 mm/yr on both paths (Figure 2). These results indicate that the CCs subsided after the 2015 phreatic eruption.

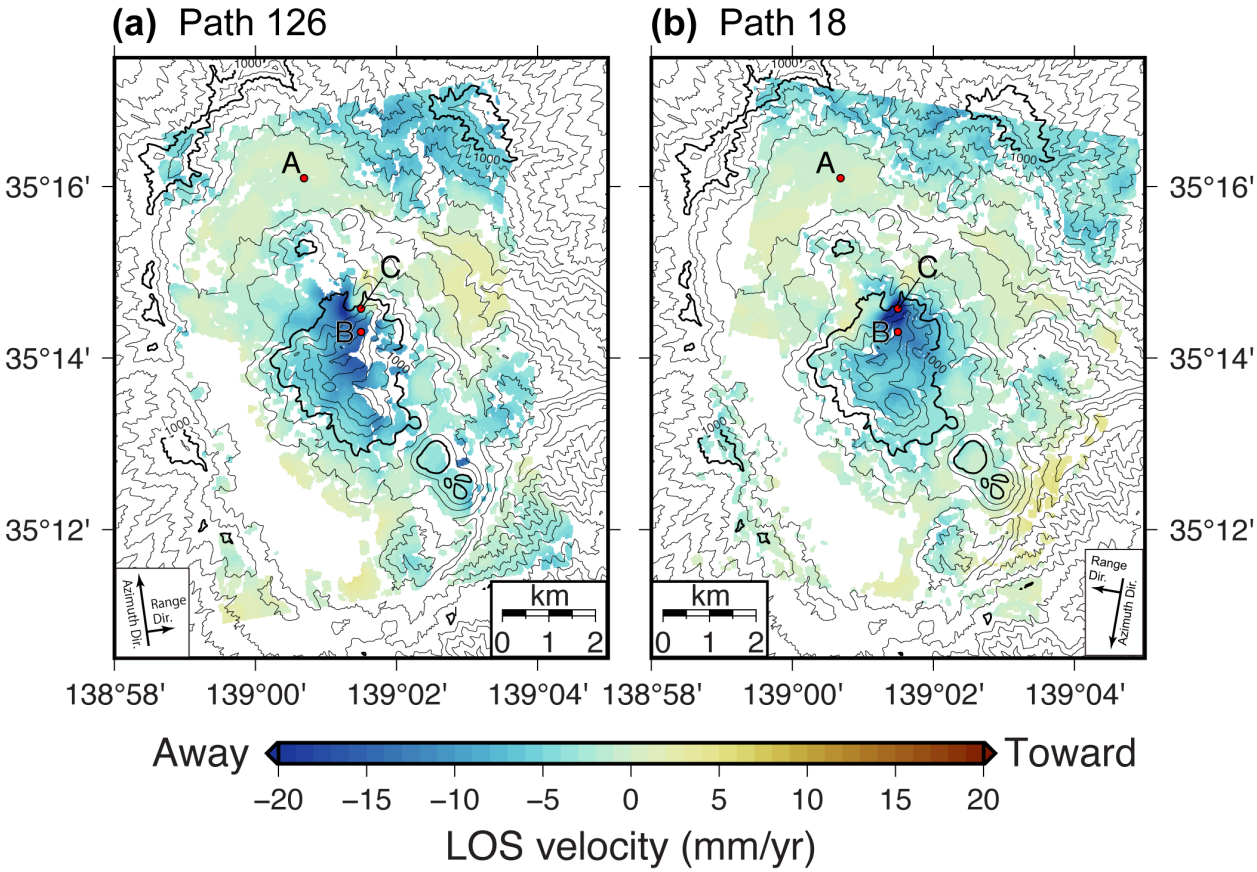

Figure 2. Distribution of LOS velocities estimated from SBAS-InSAR time series analysis of ALOS-2/PALSAR-2 data from (**a**) path 126 and (**b**) path 18. Positive and negative values indicate velocities toward and away from the satellite in the LOS direction, respectively. The contour lines represent intervals of 100 m in height. The red circles represent locations mentioned in the text and Figure 3.

Figure 3 shows the time variation of displacements at the arbitrarily selected locations A and B in Figure 2. Location A was selected in the Sengokuhara area (Figure 1), located on the caldera floor far from the CCs of the volcano, and location B was selected near the CCs. Although location A did not show any significant displacement, location B was displaced in the negative LOS direction (away from the satellite) during the analysis period. These results show that the CCs (location B) had significantly subsided with respect to location A. Assuming that the LOS displacements are entirely vertical, the vertical displacement velocity at location B is estimated to be approximately −18 to −19 mm/yr.

Significant displacement was detected near Owakudani, and this area was evaluated as location C. Location C showed the maximum velocity in the negative LOS direction on path 18 with a velocity of approximately −43 mm/yr (Figures 2(b) and 3(b)). However, the equivalent displacement was not detected on path 126 (Figure 3(a)). This velocity was considered to be due to a landslide because it shows the local displacement near Owakudani and is located on a slope steeply inclined toward the northwest (the negative LOS direction on path 18).

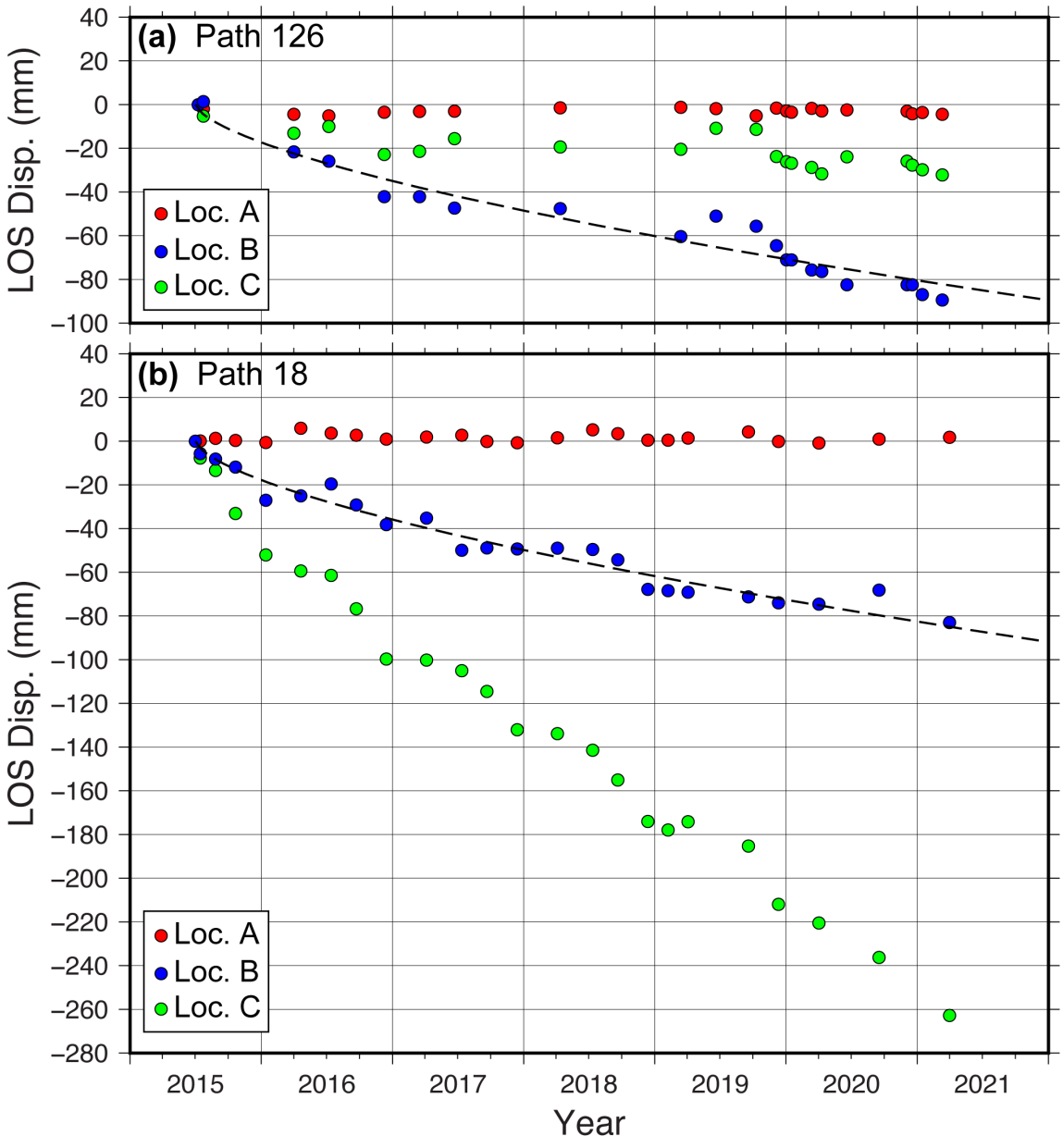

Figure 3. Time variation of the displacements at locations A–C for (**a**) path 126 and (**b**) path 18 in Figure 2. Locations A and B were arbitrarily selected on the caldera floor and the CCs of Hakone volcano, respectively. Location C is the site that shows the maximum velocity away from the satellite along the LOS in path 18. Positive and negative values indicate displacements toward and away from the satellite, respectively. Dashed lines are the lines of best fit assuming that compaction due to the pore pressure decreases (see text).

Model inversion was conducted to explain the surface velocity distributions obtained from the SBAS-InSAR time series analysis (see Text S1 and Figures S2-4). Two deflation source

models were used: a point pressure source model (Mogi, 1958) and a rectangular sill model (tensile fault model by Okada, 1985) in a semi-infinite elastic crust. The optimal parameters for each model are given in Table 1 with their standard errors. Moreover, the root mean square (RMS) and Akaike's information criterion (AIC) values for each model are also given in Table 1. The point source deflation model, which had a volume change rate of -5.96×10^4 m^3/yr, was estimated beneath the CCs of Hakone volcano at an altitude of 211.0 m above sea level. Additionally, the rectangular sill deflation model with a long side along the NW–SE direction was estimated at 95.0 m above sea level, and its opening rate was −0.111 m/yr (closing). The volume change rate of the sill deflation model was calculated to be -6.54×10^4 m^3/yr. Although the RMS and AIC values for the sill deflation model are slightly smaller than those for the point source deflation model, both models can explain the patterns of the surface velocities (Figure S2).

Table 1. *Estimated Model Parameters*.

	Model A [Point source deflation]	Model B [Sill deflation]
Longitude (°) [a]	139.0242 (0.0007)	139.0289 (0.0005) [b]
Latitude (°) [a]	35.2372 (0.0006)	35.2250 (0.0006) [b]
Altitude (m) [c]	211.0 (64.7)	95.0 (42.9)
Volume change rate (m^3/yr)	-5.96×10^4 (2.76×10^4)	-6.54×10^4 (5.78×10^3) [d]
Length (m)	–	2392.2 (94.0)
Width (m)	–	246.2 (15.4)
Strike (°)	–	339.1 (1.2)
Opening rate (m/yr)	–	−0.111 (0.005)
RMS Path 126 (mm/yr)	2.525	2.305
RMS Path 18 (mm/yr)	2.358	2.255
RMS Total (mm/yr)	2.444	2.280
AIC	3662	3574

Note: Standard errors are given in parentheses.

[a] The longitude and latitude are given in WGS-84 coordinates.

[b] The coordinates for Model B indicate the southernmost point of the sill model.

[c] The altitude is the height above sea level, corrected from the originally estimated ellipsoidal height.

[d] The volume change rate for Model B was calculated from the length, width, and opening of the sill model.

4 Discussion and Conclusion

Recent magnetotelluric surveys of Hakone volcano have reported the existence of a bell-shaped conductor (<10 Ωm) beneath the CCs of the volcano (Mannen et al., 2019; Seki et al.,

2020; Yoshimura et al., 2018). Similar bell-shaped conductors have been detected in other volcanoes (e.g., Komori et al., 2013; Nurhasan et al., 2006; Usui et al., 2017) and interpreted as impermeable layers that contain smectite, a very conductive altered mineral formed by hydrothermal activity (e.g., Lévy et al., 2018; Pellerin et al., 1996). Moreover, these impermeable layers are considered to be sealing layers that confine pressurized hydrothermal systems beneath volcanoes, which can cause phreatic eruptions (e.g., Stix & de Moor, 2018). Based on a controlled-source audio-frequency magnetotellurics (CSAMT) survey and geological analysis, Mannen et al. (2019) indicated that a portion just beneath the bell-shaped conductor forms a vapor–liquid coexisting hydrothermal system. Seki et al. (2021) showed that the bottom of the bell-shaped conductor beneath the CCs of Hakone volcano is approximately 600–700 m above sea level so that the posteruptive deflation source is located beneath the bell-shaped conductor (about 100–200 m above sea level; Figure 4). Therefore, the results of this study demonstrate that deflation has been occurring in the hydrothermal system beneath the volcano.

Based on the heat flux of 20 MW before the 2015 phreatic eruption in Owakudani (Mannen et al., 2018), the release rate for water vapor is estimated to be 2.8×10^8 kg/yr (1 atm, 100 °C). Alternatively, the deflation rates (5.96×10^4–6.54×10^4 m^3/yr) for the models in this study can be converted to water loss rates of 4.1×10^7–4.5×10^7 kg/yr, assuming the water density (690 kg/m^3) at the boiling point (311 °C) for the pore pressure at the given depth (10 MPa). This means even preeruptive water release at Owakudani was at least 6–7 times larger than the water loss of the hydrothermal system implied from our InSAR time series analysis. After the eruption, the release of water vapor can be considered to be several times greater than the preeruptive release. Therefore, the posteruptive deflation source was not regarded as the principal source of posteruptive fumarole activity, and the hydrothermal fluids are supplied from a deeper part.

So what is the cause of the posteruptive deflation in Hakone volcano? One possible cause of posteruptive deflation is compaction due to a decrease in pore pressure (Todesco et al., 2014; Wang et al., 2019). Because the behavior of crustal deformations during the 2015 phreatic eruption suggests fluid migration from the hydrothermal reservoir to a shallower edifice (Doke et al., 2018), the preeruptive pore pressure could have been released during and after the migration (Figure 4). Moreover, in the shallow part of Owakudani, a posteruptive enlargement of the high-resistivity zone (>10 Ωm) was detected (Mannen et al., 2019). This result suggests a phase change from water to vapor within the shallowest part of the hydrothermal system due to a pressure decrease after the phreatic eruption. An effect of compaction, which depends on the rheologies of subsurface rocks, can continue for a long time after a pressure drop. Todesco et al. (2014) described the process of compaction Δh with the following equation:

$$\Delta h = h_0 \frac{P_c A^{-1} t^b}{1 - \phi_0 + P_c A^{-1} t^b} \qquad (1)$$

where h_0 is the initial thickness of the compacting layer, ϕ_0 is the porosity, P_c is the pressure change, and t is the elapsed time in days. Additionally, A and b are empirically derived parameters that express the rheological properties of the compacting layer: A is a scalar associated with the magnitude of creep compaction, and b is related to the apparent viscosity of the system (Todesco et al., 2014). The initial thickness h_0 was set to 500 m, considering the structure beneath the bell-shaped conductor where the posteruptive deflation source is located (Seki et al., 2021; Figure 4), and the porosity ϕ_0 was set to 0.1 as a typical value used for

simulations of hydrothermal systems (e.g., Tanaka et al., 2018). The other parameters were estimated by fitting, assuming that the LOS displacements were entirely in the vertical direction. The values of the parameters estimated in this way are P_c = 0.91 MPa, A = 596,514 MPa·day^b, and b = 0.64, which are similar to the values estimated in Campi Flegrei (Todesco et al., 2014). The obtained curves (dashed lines in Figure 3) fit well with the pattern of subsidence after the 2015 phreatic eruption. Although the validity of these parameters remains to be verified, the results indicate that compaction due to a decrease in pore pressure is a plausible process to explain subsidence at the ground surface. Kobayashi et al. (2018) estimated a pressure increase of 0.7 MPa from the preeruptive surface displacement, which is comparable to the pressure drop during the eruption estimated in this study. Therefore, it may be that the increased pressure before the eruption was released during the eruption. However, if there are multiple hydrothermal systems in Hakone, the preeruptive pressure increase may be distinct from the co- or posteruptive pressure drop. Even so, an important point is that the InSAR observations suggest that the hydrothermal system is capable of holding this level of excess pressure.

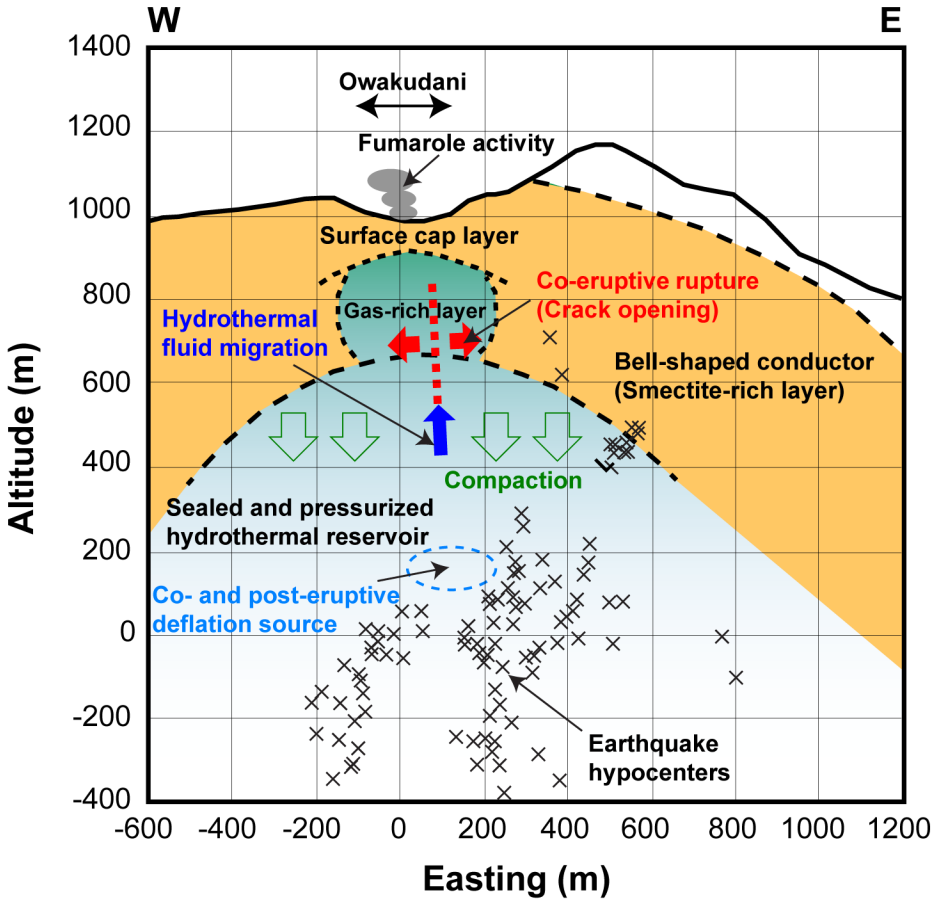

Figure 4. Schematic illustration of the shallow hydrothermal system beneath the CCs of Hakone volcano. The subsurface model is based on the conductivity structure and interpretation shown in Figure 4 of Seki et al. (2021), previous deformation sources proposed by Doke et al. (2018), and the results of the present study. During the 2015 phreatic eruption, the sealing layer was ruptured, and pressurized hydrothermal fluids migrated toward the shallower edifice.

Posteruptive deflation might be caused by a pore pressure decrease in the hydrothermal reservoir due to fluid migration.

Another possible cause of deflation is a thermoelastic response with cooling (e.g., Furuya, 2005; Wang and Aoki, 2019). However, most examples of thermoelastic responses are related to the cooling of intruding magma bodies. Narita et al. (2019) demonstrated that the temperature change in the thermoelastic response expected from the posteruptive deflation after the 2014 phreatic eruption of Ontake volcano, Japan, was too large for the shallow part (500 m in depth) of the volcano. They concluded that the thermoelastic response is not a major factor contributing to deflation in Ontake volcano. The 2015 phreatic eruption of Hakone volcano was very small in scale, and significant temperature changes were unlikely to have happened in the coexisting vapor–liquid hydrothermal system, where the temperature change was buffered by the release of latent heat due to the condensation of water vapor (e.g., Ingebritsen et al., 2006). Therefore, the thermoelastic process is unlikely to be a major factor in the deflation of Hakone volcano.

When considering compaction due to a decrease in pore pressure, this deflation process is expected to continue for a long period, in accordance with Equation (1), unless there is a particular change in pressure conditions. However, if the sealing ability is restored as a result of mineral crystallization or other factors and the pressure starts to increase, this deflation will stop early. Therefore, it is important to monitor the displacement at the ground surface to assess the pressure conditions of the hydrothermal system and the risk of future phreatic eruptions.

Acknowledgments, Samples, and Data

We would like to thank Dr. Teruyuki Kato of Taisho University for his helpful comments. This research was funded by JSPS KAKENHI grant numbers 19K04005 and 21H04602. ALOS-2/PALSAR-2 data were provided by JAXA via the Coordinating Committee for the Prediction of Volcanic Eruption as part of the Volcano Working Group project, “ALOS Domestic Demonstration on Disaster Management Application.” The original ALOS-2/PALSAR-2 data belong to JAXA and can be purchased from RESTEC (https://www.restec.or.jp/en/). The processed data and geodetic modeling results are available on Zenodo (https://doi.org/10.5281/zenodo.5014834).

References

Berardino, P., Fornaro, G., Lanari, R., & Sansosti, E. (2002). A new algorithm for surface deformation monitoring based on small baseline differential SAR interferograms. *IEEE Transactions on Geoscience and Remote Sensing*, *40*(11), 2375–2383. https://dx.doi.org/10.1109/TGRS.2002.803792

Costantini, M. (1998). A novel phase unwrapping method based on network programming. *IEEE Transactions on Geoscience and Remote Sensing*, *36*(3), 813–821. https://dx.doi.org/10.1109/36.673674

Doke, R., Harada, M., Mannen, K., Itadera, K., & Takenaka, J. (2018). InSAR analysis for detecting the route of hydrothermal fluid to the surface during the 2015 phreatic eruption of Hakone Volcano, Japan. *Earth, Planets and Space*, *70*, 63. https://dx.doi.org/10.1186/S40623-018-0834-4

Fournier, R.O. (1999). Hydrothermal processes related to movement of fluid from plastic into brittle rock in the magmatic-epithermal environment. *Economic Geology*, *94*(8), 1193–1211. https://dx.doi.org/10.2113/gsecongeo.94.8.1193

Furukawa, R., Ishizuka, Y., Yamasaki, S., Mannen, K., Nagai, M., Miwa, T., et al. (2015). Pyroclastic fall deposit of 2015 eruption from Hakone volcano, Japan. *Programme and Abstracts the Volcanological Society of Japan*, *2015*, P93. https://dx.doi.org/10.18940/vsj.2015.0_191 (in Japanese)

Furuya, M. (2005). Quasi-static thermoelastic deformation in an elastic half-space: Theory and application to InSAR observations at Izu-Oshima volcano, Japan. *Geophysical Journal International*, *161*(1), 230–242. https://dx.doi.org/10.1111/j.1365-246x.2005.02610.x

Geological Society of Japan (2007). *Geological leaflet 1 Hakone Volcano.* Tokyo: Geological Society of Japan. (in Japanese)

Goldstein, R.M., & Werner, C.L. (1998). Radar interferogram filtering for geophysical applications. *Geophysical Research Letters*, *25*(21), 4035–4038. https://dx.doi.org/10.1029/1998gl900033

Hamling, I.J., Williams, C.A., & Hreinsdóttir, S. (2016). Depressurization of a hydrothermal system following the August and November 2012 Te Maari eruptions of Tongariro, New Zealand. *Geophysical Research Letters*, *43*(1), 168–175. https://dx.doi.org/10.1002/2015gl067264

Harada, M., Doke, R., Mannen, K., Itadera, K., & Satomura, M. (2018). Temporal changes in inflation sources during the 2015 unrest and eruption of Hakone volcano, Japan. *Earth, Planets and Space*, *70*, 152. https://dx.doi.org/10.1186/S40623-018-0923-4

Himematsu, Y., Ozawa, T., & Aoki, Y. (2020). Coeruptive and posteruptive crustal deformation associated with the 2018 Kusatsu-Shirane phreatic eruption based on PALSAR-2 time series analysis. *Earth, Planets and Space*, *72*, 116. https://dx.doi.org/10.1186/s40623-020-01247-6

Honda, R., Yukutake, Y., Morita, Y., Sakai, S. I., Itadera, K., & Kokubo, K. (2018). Precursory tilt changes associated with a phreatic eruption of the Hakone volcano and the corresponding source model. *Earth, Planets and Space*, *70*, 117. https://dx.doi.org/10.1186/s40623-018-0887-4

Ingebritsen, S.E., Sanford, W.E., & Neuzil, C.E. (2006). *Groundwater in geologic processes, 2nd edition*. Cambridge: Cambridge University Press.

Kobayashi, M. (2008). Eruption History of the Hakone Central Cone Volcanoes, and Geographical Development Closely Related to Eruptive Activity in the Hakone Caldera. *Research Report of the Kanagawa Prefectural Museum, Natural History*, *13*, 43–60. (in Japanese with English abstract)

Kobayashi, M., Mannen, K., Okuno, M., Nakamura, T., & Hakamata, K. (2006). The Owakidani tephra group: A newly discovered post-magmatic eruption product of Hakone Volcano, Japan. *Bulletin of the Volcanological Society of Japan*, *51*, 245–256. https://doi.org/10.18940/kazan.51.4_245 (in Japanese with English Abstract)

Kobayashi, T., Morishita, Y., & Munekane, H. (2018). First detection of precursory ground inflation of a small phreatic eruption by InSAR. *Earth and Planetary Science Letters*, *491*, 244–254. https://dx.doi.org/10.1016/j.epsl.2018.03.041

Komori, S., Kagiyama, T., Utsugi, M., Inoue, H., & Azuhata, I. (2013). Two-dimensional resistivity structure of Unzen Volcano revealed by AMT and MT surveys. *Earth, Planets and Space*, *65*(7), 759–766. https://dx.doi.org/10.5047/eps.2012.10.005

Lévy, L., Gibert, B., Sigmundsson, F., Flóvenz, Ó., Hersir, G., Briole, P., & Pezard, P. (2018). The role of smectites in the electrical conductivity of active hydrothermal systems: Electrical properties of core samples from Krafla volcano, Iceland. *Geophysical Journal International*, *215*(3), 1558–1582. https://dx.doi.org/10.1093/gji/ggy342

Mannen, K., Abe, Y., Daita, Y., Doke, R., Harada, M., Kikugawa, G., et al. (2021). Volcanic unrest at Hakone volcano after the 2015 phreatic eruption: Reactivation of a ruptured hydrothermal system? *Earth, Planets and Space*, *73*, 80. https://dx.doi.org/10.1186/s40623-021-01387-3

Mannen, K., Tanada, T., Jomori, A., Akatsuka, T., Kikugawa, G., Fukazawa, Y., et al. (2019). Source constraints for the 2015 phreatic eruption of Hakone volcano, Japan, based on geological analysis and resistivity structure. *Earth, Planets and Space*, *71*, 135. https://dx.doi.org/10.1186/s40623-019-1116-5

Mannen, K., Yukutake, Y., Kikugawa, G., Harada, M., Itadera, K., & Takenaka, J. (2018). Chronology of the 2015 eruption of Hakone volcano, Japan: Geological background, mechanism of volcanic unrest and disaster mitigation measures during the crisis. *Earth, Planets and Space*, *70*, 68. https://dx.doi.org/10.1186/s40623-018-0844-2

Mogi, K. (1958). Relations between the eruptions of various volcanoes and the deformations of the ground surfaces around them. *Bulletin of the Earthquake Research Institute*, *36*, 99–134.

Narita, S., & Murakami, M. (2018). Shallow hydrothermal reservoir inferred from post-eruptive deflation at Ontake Volcano as revealed by PALSAR-2 InSAR. *Earth, Planets and Space*, *70*, 191. https://dx.doi.org/10.1186/s40623-018-0966-6

Narita, S., Murakami, M., & Tanaka, R. (2019). Quantitative relationship between plume emission and multiple deflations after the 2014 phreatic eruption at Ontake volcano, Japan. *Earth, Planets and Space*, *70*, 145. https://dx.doi.org/10.1186/s40623-019-1124-5

Nurhasan, Ogawa, Y., Ujihara, N., Tank, S.B., Honkura, Y., Onizawa, S.Y., et al. (2006). Two electrical conductors beneath Kusatsu–Shirane volcano, Japan, imaged by audiomagnetotellurics, and their implications for the hydrothermal system. *Earth, Planets and Space*, *58*(8), 1053–1059. https://dx.doi.org/10.1186/bf03352610

Okada, Y. (1985). Surface deformation due to shear and tensile faults in a half-space. *Bulletin of the Seismological Society of America*, *75*(4), 1135–1154.

Pavlis, N.K., Holmes, S.A., Kenyon, S.C., & Factor, J.K. (2012). The development and evaluation of the Earth Gravitational Model 2008 (EGM2008). *Journal of Geophysical Research: Solid Earth*, *117*(B4). https://dx.doi.org/10.1029/2011JB008916

Pellerin, L., Johnston, J.M., & Hohmann, G.W. (1996). A numerical evaluation of electromagnetic methods in geothermal exploration. *Geophysics*, *61*(1), 121–130. https://dx.doi.org/10.1190/1.1443931

Rosenqvist, A., Shimada, M., Suzuki, S., Ohgushi, F., Tadono, T., Watanabe, M., et al. (2014). Operational performance of the ALOS global systematic acquisition strategy and observation plans for ALOS-2 PALSAR-2. *Remote Sensing of Environment*, *155*, 3–12. https://doi.org/10.1016/j.rse.2014.04.011

Seki, K., Kanda, W., Mannen, K., Takakura, S., Koyama, T., Noguchi, R., et al. (2021). Imaging the Source Region of the 2015 Phreatic Eruption at Owakudani, Hakone Volcano, Japan, Using High-Density Audio-Frequency Magnetotellurics. *Geophysical Research Letters*, *48*(1). https://dx.doi.org/10.1029/2020gl091568

Stix, J., & De Moor, J.M. (2018). Understanding and forecasting phreatic eruptions driven by magmatic degassing. *Earth, Planets and Space*, *70*, 83. https://dx.doi.org/10.1186/s40623-018-0855-z

Tanaka, R., Hashimoto, T., Matsushima, N., & Ishido, T. (2018). Contention between supply of hydrothermal fluid and conduit obstruction: inferences from numerical simulations. *Earth, Planets and Space*, *70*, 72. https://dx.doi.org/10.1186/s40623-018-0840-6

Todesco, M., Costa, A., Comastri, A., Colleoni, F., Spada, G., & Quareni, F. (2014). Vertical ground displacement at Campi Flegrei (Italy) in the fifth century: Rapid subsidence driven by pore pressure drop. *Geophysical Research Letters*, *41*(5), 1471–1478. https://dx.doi.org/10.1002/2013gl059083

Tsuchiya, M., Mannen, K., Kobayashi, M., & Fukuoka, T. (2017). Two Types of Glass Shards within the Owakidani Tephra Group Deposit, Hakone Volcano: Constraints on Their Sources and Ages. *Bulletin of the Volcanological Society of Japan*, *62*(1), 23–30. https://dx.doi.org/10.18940/kazan.62.1_23 (in Japanese with English Abstract)

Usui, Y., Ogawa, Y., Aizawa, K., Kanda, W., Hashimoto, T., Koyama, T., et al. (2017). Three-dimensional resistivity structure of Asama Volcano revealed by data-space magnetotelluric inversion using unstructured tetrahedral elements. *Geophysical Journal International*, *208*(3), 1359–1372. https://dx.doi.org/10.1093/gji/ggw459

Wang, X., & Aoki, Y. (2019). Posteruptive Thermoelastic Deflation of Intruded Magma in Usu Volcano, Japan, 1992–2017. *Journal of Geophysical Research: Solid Earth*, *124*(1), 335–357. https://dx.doi.org/10.1029/2018jb016729

Wang, X., Aoki, Y., & Chen, J. (2019). Surface deformation of Asama volcano, Japan, detected by time series InSAR combining persistent and distributed scatterers, 2014–2018. *Earth, Planets and Space*, *70*, 121. https://dx.doi.org/10.1186/s40623-019-1104-9

Yoshimura, R., Ogawa, Y., Yukutake, Y., Kanda, W., Komori, S., Hase, H., et al. (2018). Resistivity characterisation of Hakone volcano, Central Japan, by three-dimensional magnetotelluric inversion. *Earth, Planets and Space*, *70*, 66. https://dx.doi.org/10.1186/s40623-018-0848-y

Yukutake, Y., Abe, Y., & Doke, R. (2019). Deep Low-Frequency Earthquakes Beneath the Hakone Volcano, Central Japan, and their Relation to Volcanic Activity. *Geophysical Research Letters*, *46*(20), 11035–11043. https://dx.doi.org/10.1029/2019gl084357

Yukutake, Y., Honda, R., Harada, M., Doke, R., Saito, T., Ueno, T., et al. (2017). Analyzing the continuous volcanic tremors detected during the 2015 phreatic eruption of the Hakone volcano. *Earth, Planets and Space*, *69*, 164. https://dx.doi.org/10.1186/S40623-017-0751-Y

References From the Supporting Information

Jonsson, S. (2002). Fault Slip Distribution of the 1999 Mw 7.1 Hector Mine, California, Earthquake, Estimated from Satellite Radar and GPS Measurements. *Bulletin of the Seismological Society of America*, *92*(4), 1377–1389. https://dx.doi.org/10.1785/0120000922

Marquardt, D.W. (1963). An Algorithm for Least-Squares Estimation of Nonlinear Parameters. *Journal of the Society for Industrial and Applied Mathematics*, *11*(2), 431–441. https://dx.doi.org/10.1137/0111030

438 Mogi, K. (1958). Relations between the eruptions of various volcanoes and the deformations of
439 the ground surfaces around them. *Bulletin of the Earthquake Research Institute*, *36*, 99–
440 134.
441 Okada, Y. (1985). Surface deformation due to shear and tensile faults in a half-space. *Bulletin of*
442 *the Seismological Society of America*, *75*(4), 1135–1154.
443 Welstead, S. (1999). *Fractal and Wavelet Image Compression Techniques (Vol. TT40)*.
444 Bellingham, Washington: SPIE Optical Engineering Press.
445